Aratyn-Schaus et al., http://www.jcb.org/cgi/content/full/jcb.201508026/DC1

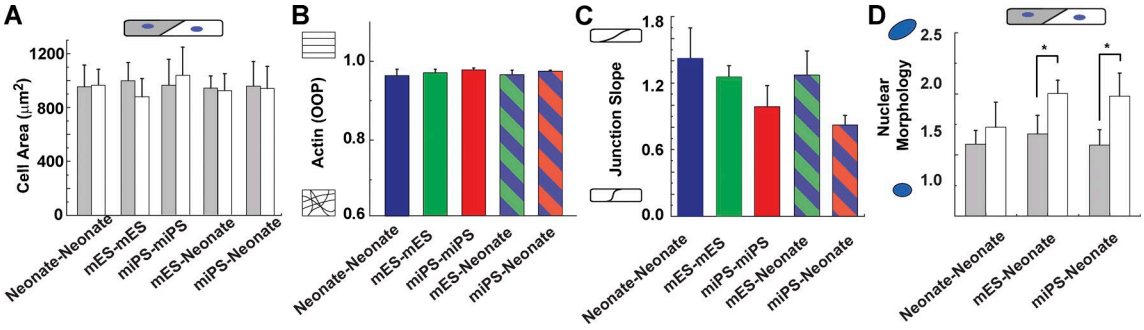

Figure S1. **Quantitative characterization of cell morphology in homogeneous and heterogeneous μtissues.** A variety of morphological parameters were assessed in individual cells as a function of μtissue type. (A) Surface area (n = 14, 9, 12, 8, and 9 for neonate-neonate, mES-mES, mES-neonate, miPS-miPS, and miPS-neonate, respectively). (B) Actin OOP (n = 8, 8, 6, 4, and 8 for neonate-neonate, mES-mES, mES-neonate, miPS-miPS, and miPS-neonate, respectively). (C) Slope of the cell–cell junction (n = 11, 6, 10, 6, and 9 for neonate-neonate, mES-mES, mES-neonate, miPS-miPS, and miPS-neonate, respectively). (D) Nuclear eccentricity (n = 5 for all μtissues). Results presented as mean ± SEM. *, P < 0.05.

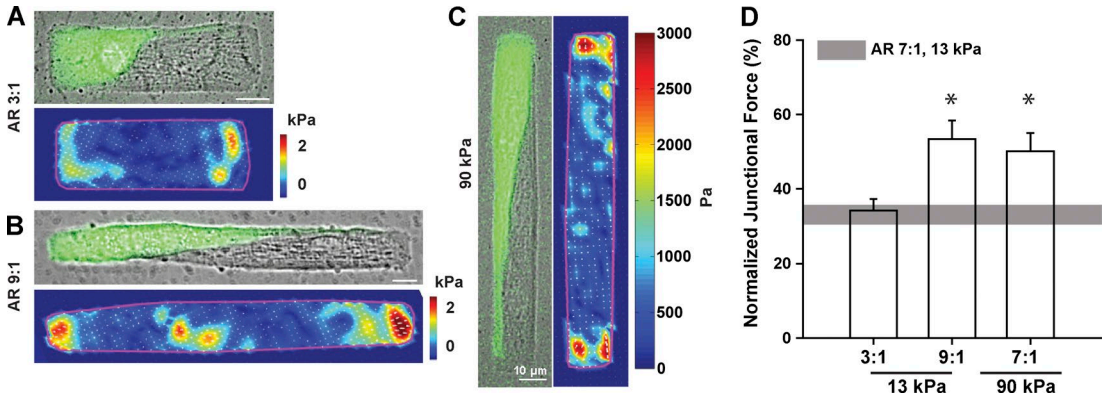

Figure S2. **Junctional forces in heterogeneous μtissues in disease-mimicking microenvironments.** (A and B) DIC (top) and traction force field (bottom) images of mES-derived (green) and neonate cardiomyocytes seeded on fibronectin-coated islands with length-to-width ratios of 3:1 (A) and 9:1 (B), mimicking concentric and eccentric hypertrophy, respectively. (C) DIC (left) and traction force field (right) images of mES-derived (green) and neonate cardiomyocytes seeded on fibronectin islands with length-to-width ratios of 7:1, microcontact-printed on a stiff (90 kPa) substrate, representing a fibrotic microenvironment. (D) Summary statistics show that the percentage of the peak systolic traction force dissipated at the cell–cell junction in pathological conditions (3:1, 9:1, 7:1 at 90 kPa) is similar to or greater than that observed in physiological conditions (7:1 at 13 kPa; Fig. 2, gray box). This is in agreement with previous studies (McCain, 2012, 2014). Results are mean ± SEM (n = 13, 6, and 7 for 3:1, 9:1, and 90 kPa, respectively). *, P < 0.05.

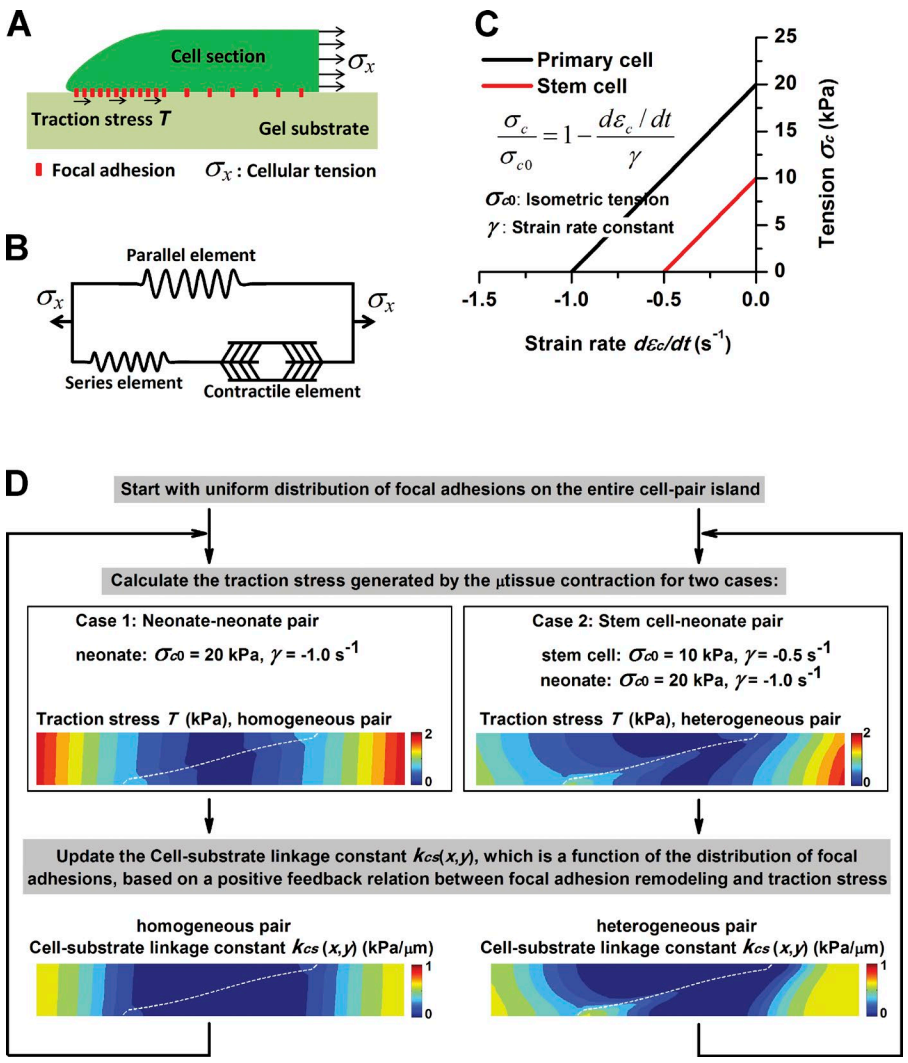

Figure S3. **Computational mechanics and finite element simulations.** (A) A section of the μtissue depicting the cellular tension along the longitudinal direction and the traction stress on the gel substrate. (B) Hill's three-element model for muscle contraction. (C) Linearized stress–strain rate relation (i.e., the inset equation) for the contractile element of Hill's three-element model. (D) Schematic for determining the cell substrate linkage constant in the steady state using a positive feedback between the focal adhesion maturation and traction stress.

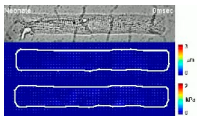

Video 1. **Spontaneous contraction of an isolated neonate myocyte.** Time course of the spontaneous contraction of an individual microcontact-printed mouse neonate ventricular myocyte adhered to compliant hydrogel, visualized by DIC imaging (top). Corresponding substrate displacement (middle) and traction stress (bottom) heat maps resulting from TFM. Solid white outline indicates cellular boundary.

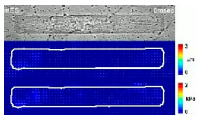

Video 2. **Spontaneous contraction of an isolated mES-CM.** Time course of the spontaneous contraction of an individual microcontact-printed mES-CM adhered to compliant hydrogel, visualized by DIC imaging (top). Corresponding substrate displacement (middle) and traction stress (bottom) heat maps resulting from TFM. Solid white outline indicates cellular boundary.

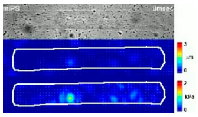

Video 3. **Spontaneous contraction of an isolated miPS-CM.** Time course of the spontaneous contraction of an individual microcontact-printed miPS-CM adhered to compliant hydrogel, visualized by DIC imaging (top). Corresponding substrate displacement (middle) and traction stress (bottom panel) heat maps resulting from TFM. Solid white outline indicates cellular boundary.

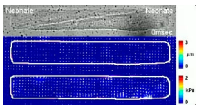

Video 4. **Spontaneous contraction of coupled neonate myocytes.** Time course of the spontaneous contraction of a microcontact-printed μtissue composed of a pair of mouse neonate ventricular myocytes adhered to compliant hydrogel, visualized by DIC imaging (top). Corresponding substrate displacement (middle) and traction stress (bottom) heat maps resulting from TFM. Solid white outline indicates cellular boundary.

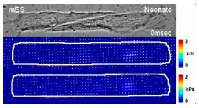

Video 5. **Spontaneous contraction of a coupled neonate myocyte and mES-CMs.** Time course of the spontaneous contraction of a microcontact-printed μtissue composed of a coupled mES-CM and a mouse neonate ventricular myocyte adhered to compliant hydrogel, visualized by DIC imaging (top). Corresponding substrate displacement (middle) and traction stress (bottom) heat maps resulting from TFM. Solid white outline indicates cellular boundary.

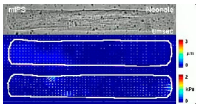

Video 6. **Spontaneous contraction of a coupled neonate myocyte and miPS-CM.** Time course of the spontaneous contraction of a microcontact-printed μtissue composed of a coupled miPS-CM and a mouse neonate ventricular myocyte adhered to compliant hydrogel, visualized by DIC imaging (top). Corresponding substrate displacement (middle) and traction stress (bottom) heat maps resulting from TFM. Solid white outline indicates cellular boundary.

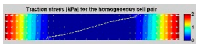

Video 7. **Time course of the simulated traction stress for the homogeneous cell pair using the finite element model.** High stress is located at the two ends of the island.

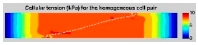

Video 8. **Time course of the simulated cellular tension for the homogeneous cell pair using the finite element model.** Cellular tension is uniform within the μtissue except at the two ends.

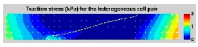

Video 9. **Time course of the simulated traction stress for the heterogeneous cell pair using the finite element model.** High traction stress also happens at the cell–cell junction near the tip of the neonate cell.

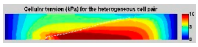

Video 10. **Time course of the simulated cellular tension for the heterogeneous cell pair using the finite element model.** Cellular tension is not uniform even in the middle region of the μtissue.

References

McCain, M.L., H. Lee, Y. Aratyn-Schaus, A.G. Kléber, and K.K. Parker. 2012. Cooperative coupling of cell-matrix and cell-cell adhesions in cardiac muscle. *Proc. Natl. Acad. Sci. USA.* 109:9881–9886. http://dx.doi.org/10.1073/pnas.1203007109

McCain, M.L., H. Yuan, F.S. Pasqualini, P.H. Campbell, and K.K. Parker. 2014. Matrix elasticity regulates the optimal cardiac myocyte shape for contractility. *Am. J. Physiol. Heart Circ. Physiol.* 306:H1525–H1539. http://dx.doi.org/10.1152/ajpheart.00799.2013